23rd ABCM International Congress of Mechanical Engineering
December 6-11, 2015, Rio de Janeiro, RJ, Brazil

AN OPTIMIZED CONCENTRATED PARAMETERS SYSTEM APPROACH TO DRILL STRING DYNAMICS MODELING

Adriano Domeny
Hans Ingo Weber
Pontifícia Universidade Católica do Rio de Janeiro. Marquês de São Vicente Street, 225, Gávea, CEP 22453900, Rio de Janeiro - RJ, Brazil
adrianodomeny@gmail.com

Abstract. *In order to better understand the dynamic behavior of a drillstring subjected to various electrical and mechanical excitations, torsional effects will be investigated separately. An optimized concentrated parameters model was proposed based on a test bench made up by a double torsional pendulum, coupled to a DC motor by means of a planetary gearbox. The double pendulum is made up of metallic rotors driven by a very slender steel shaft, one at the extremity of the shaft and the other in an intermediate position. The shaft is fixed to the output of the gearbox connected to the DC motor. The rotors, on the other hand, are supported on roller bearings by a rigid frame, in a way to separate possible flexural vibrations from the torsional vibrations that shall be investigated. In the proposed model for the coupled electro-mechanical system, the torsional system is composed by the slender shaft, both inertias, one modeling the outer rotor and the other the inner one, and the engine rotor fixed to the shaft by means of the gearbox. It was represented by an optimized concentrated parameters mathematical model with a predetermined number of degrees of freedom. The modes of vibration were a priori calculated analytically from a similar continuous model based on the torsional wave equation of the shaft. For validation purposes, some dynamic responses of the system were superimposed, obtained both, by numerical simulation of the proposed mode as well as by experimental tests. The complexity of this model is easily increased and the techniques explored in this paper to define optimal parameters for the model can be valuable for engineering applications.*

Keywords: *drilling system, concentrated parameters, optimization*

1. INTRODUCTION

In general the drilling system used in oil and gas industries is constituted among other elements by an electric or hydraulic motor, which provides rotation energy to a bit by means of a hollow steel cylindrical column, called drillstring, which in turn is stretched along all its extension. The BHA - Bottom Hole Assembly - is located at the end of the drillstring. It is a more robust cylindrical structure designed to perform in compression regime, and is responsible, among other things, for the stability of the drilling process, for keeping the drill string stretched, and mainly, for generating pressure on the bit-rock interaction.

The drilling system can be understood in a more simplified way, as a mechanical system constituted by a motor and by a torsional system subjected to various types of mechanical excitations: the bit-rock interaction, friction in contact of the torsional system with wall of the hole, impacts with the wall of the hole, and friction due to the drill fluid. These excitations generate various types of vibration in the system, which constitute in the overall the main factor of loss in the effectiveness of the bit penetration during drilling, and the premature fault of certain mechanical components (Franca, 2004). On the other hand, there is a consensus that the main source of friction is the BHA in its interaction with the hole (Pogorelov *et al.*, 2012).

In view of all these phenomena, the computational model for the system dynamics has been an important tool to better understand its behavior, in order to mitigate the vibrational effects. Following this line of thought, Andrade (2013) used a bench with a motor coupled to a simple torsional pendulum, equipped with a disk brake system. In his formulation, he used the method of concentrated parameters, inserting new parameters until the convergence of the third natural frequency is obtained. In turn, Mihajlovic (2005) adopted a similar bench, through which he sought to validate the model proposed by him, and the coupling of the lateral and torsional dynamics were considered. FEM was used in his formulation.

The current article proposes an optimized concentrated parameters model for a bench constituted by a DC motor coupled to a double torsional pendulum. The torsional system of the model is composed by the slender shaft, both inertias of the double pendulum, one modeling the outer rotor and the other the inner one; and by the engine rotor fixed to the shaft by means of a planetary gearbox. The rotors, on the other hand, are supported on roller bearings by a rigid frame, in a way to separate possible flexural vibrations from the torsional vibrations that shall be investigated. Firstly a description of the bench was accomplished. Next, the methodology for obtaining the parameters was presented. Finally the experimental test accomplished for the model validation was described, and the results were analyzed.

2. MATHEMATICAL MODEL

The bench is constituted by a coupled DC motor, by means of a mechanical reduction box, to a double torsional pendulum, which in turn is made up of a steel shaft, of length l and diameter d. The outer steel rotor and the inner one have moments of inertia J_1 and J_2, respectively. The inner rotor is a distance l_1 from the end of the motor. Figure 1 presents a schematic model of the bench, and Tab. 1 presents its parameters with their respective values.

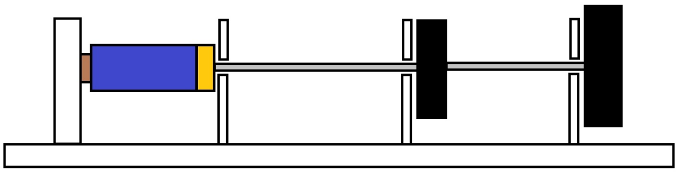

Figure 1. Schematic model of bench.

Table 1. Bench Parameters.

Parameters	Symbol	Numerical Values
Inertia of the drive rotor $(kg*m^2)^{(1)}$	J_m	$4.698*10^{-4}$
Motor inductance $(H)^{(1)}$	L	$8.437*10^{-4}$
Motor damping coefficient $(kg*m^2/s)^{(1)}$	C_m	$1.784*10^{-4}$
Reduction in drive autput $^{(1)}$	n_R	8
Motor parameter $(Nm/A)^{(1)}$	k_t	0.126
Motor parameter $(V/(rad/s))^{(1)}$	k_e	0.0588
Length of the metal shaft (m)	l	2.430
Distance between the second rotor and the drive (m)	l_1	1.742
Moment of inertia of the rotor 1 $(kg*m^2)$	J_1	0.0276
Moment of inertia of the rotor 2 $(kg*m^2)$	J_2	0.0153
Steel density (kg/m^3)	ρ	7850
Steel shear coefficient (GPa)	G	78.9
Shaft diameter (mm)	d	3
Distributed damping coefficient $(kg*m/s)$	D	0.007
Friction model parameter	α_s	5.0
Friction model parameter	λ_s	0.9
Friction model parameter (rad/s)	ω_0	0.0001π
Kinetic friction torque of the J_1 rotor bearing (Nm)	$T_{S_{0_1}}$	0.0256
Kinetic friction torque of the J_2 rotor bearing (Nm)	$T_{S_{0_2}}$	0.0071
Kinetic friction torque of the engine rotor bearing (Nm)	$T_{S_{0_3}}$	2.1678

$^{(1)}$ DC Motor manual: ENGEL GNM $5480 - G6.1$

The equations of the theoretical model of the bench were derived from Lagrange equations for a coupled electromechanical system, considering the vector of generalized coordinates $\mathbf{z} = \begin{bmatrix} \theta & q \end{bmatrix}^T$, where $\theta = \begin{bmatrix} \theta_1 & \theta_2 & \cdots & \theta_N \end{bmatrix}^T$ is the vector of angular displacements of the torsional pendulum, and q the electric charges of the motor.

2.1 Bench Model

Equation (1) shows the final dimensionless expression of the dynamic model of the coupled electromechanical system, considering that N is the number of degrees of freedom of the torsional system concentrated parameters model.

$$\begin{bmatrix} \ddot{\theta}^* \\ \ddot{q}^* \end{bmatrix} + \begin{bmatrix} \mathbf{C}^* & \alpha^* \\ \beta^* & \sigma^* \end{bmatrix} \begin{bmatrix} \dot{\theta}^* \\ \dot{q}^* \end{bmatrix} + \begin{bmatrix} \mathbf{K}^* & \mathbf{0} \\ \mathbf{0} & 0 \end{bmatrix} \begin{bmatrix} \theta \\ q^* \end{bmatrix} + \left(\frac{T^2}{\rho J l}\right) \mathbf{T_{clamp_1}} + \left(\frac{T^2}{\rho J l}\right) \mathbf{T_{S_{1,2,3}}} = \begin{bmatrix} \mathbf{0} \\ \sigma^* \end{bmatrix} v_A^* \quad (1)$$

The term $\mathbf{T_{clamp_1}}$, explained in Eq. (2), corresponds to an applied clamping torque on rotor J_1, from an instant t_r in regime until the predetermined time instant t_c. The term deg refers to the step function, and T_{ext_1} is the total torque applied on rotor J_1, except for $\mathbf{T_{clamp_1}}$. The general term $\mathbf{I_{D_i}^{(N+1)}}$ refers to the $i-$th column of the identity matrix of dimension $N+1$.

$$\mathbf{T_{clamp_1}} = \Big(T_{ext_1} + K_{clamp_1}(\dot{\theta}_N)\Big)\, \mathbf{I_{D_N}^{(N+1)}} \Big(\deg(t^* - t_r^*) - \deg(t^* - t_c^*)\Big) \tag{2}$$

The term $\mathbf{T_{S_{1,2,3}}}$, explained in Eq. (3), refers to dry friction torque in the bearings that support the rotors J_1, J_2 and J_m. The term $N_1 = \left\lfloor \frac{l_1}{l}(N-1) \right\rfloor$ was defined in such a way that θ_{N_1+1} corresponds to the angular position of J_2. The terms $J = \pi d^4/4$ and $T = l/c_p$ correspond to, respectively, the moment of inertia of the shaft and the used time scale, where $c_p = \sqrt{G/\rho}$. The term v_A^* correspond to the dimensionless input voltage.

$$\mathbf{T_{S_{1,2,3}}} = T_{S_1}(\omega_N)\mathbf{I_{D_N}^{(N+1)}} + T_{S_2}(\omega_{N_1+1})\mathbf{I_{D_{N_1+1}}^{(N+1)}} + T_{S_3}(\omega_{\mathbf{1}})\mathbf{I_{D_1}^{(N+1)}} \tag{3}$$

The model of the friction torque is shown in Eq. (4), where Ψ_2 is a dimensionless function (Eq. (5)).

$$T_{S_i}(\omega) = T_{S_{0_i}} \Psi_2(\omega/\omega_{0_i}) \tag{4}$$

$$\Psi_2(\eta) = \begin{cases} -\lambda_s + (\lambda_s - B)\exp(\alpha_s \eta) & , \eta \leq -\eta_1 \\ -\frac{1}{2}\eta^3 + \frac{3}{2}\eta & , -\eta_1 \leq \eta \leq \eta_1 \\ \lambda_s + (B - \lambda_s)\exp(-\alpha_s \eta) & , \eta_1 \leq \eta \end{cases} \tag{5}$$

The terms α_s, λ_s and ω_0 are predetermined parameters of the friction model (Tab. 1), η_1 is a calculated parameter as the limit of the sequence η_n explained in Eq. (6), and B a fourth parameter calculated through Eq. (7).

$$\begin{cases} \eta_{n+1} = \eta_n - \frac{\eta_n^3 + \frac{3}{\alpha}\eta_n^2 - 3\eta_n + \left(2\lambda - \frac{3}{\alpha_s}\right)}{3\eta_n^2 + \frac{6}{\alpha_s}\eta_n - 3} \\ \eta_0 = \frac{1+\sqrt{3}}{2} \end{cases} \tag{6}$$

$$B = \lambda_s + \frac{3}{2\alpha_s}(\eta_1^2 - 1)\exp(\alpha_s \eta_1) \tag{7}$$

Figure 2 shows the curve of function Ψ_2.

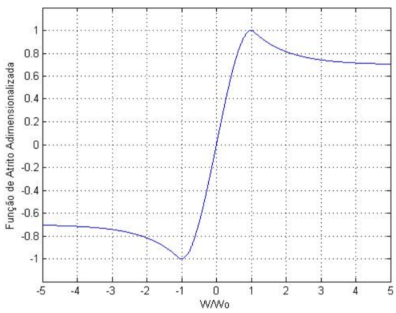

Figure 2. Dimensionless Friction Model

The terms α^*, β^*, σ^*, $\mathbf{C}^*$, $\mathbf{K}^*$, from Eq. (1), are explained in Eq. (8), Eq. (9), Eq. (10), Eq. (11) and Eq. (12), respectively, where $\gamma_i = \frac{I_i}{\rho J l}$ is the dimensionless inertia associated to θ_i. Particularly, $I_1 = n_R^2 J_m$, $I_{N_1+1} = J_2$ e $I_N = J_1$. Finally, $x_i^* = x_i/l$ corresponds to the dimensionless position of inertia I_i on the shaft, considering $x = 0$ for the end of the drive.

Table 2 shows a list of the main parameters of the model with the respective dimensionless variable.

Table 2. Main Dimensionless Variables.

Variable	Dimensionless Variable
x	$x^* = \frac{x}{l}$
t	$t^* = \frac{t}{T}$
v_A	$v_A^* = \frac{v_A}{2\pi k_e}$
$i_A = \dot{q}$	$i_A^* = i_A \frac{R}{2\pi k_e}$
q	$q^* = q\frac{1}{T}\frac{R}{2\pi k_e}$

$$\alpha^* = \begin{bmatrix} -\frac{n_R k_t T}{\rho J l \gamma_1} & 0 & \dots & 0 \end{bmatrix}^T \tag{8}$$

$$\beta^* = \begin{bmatrix} \frac{n_R R}{2\pi L} & 0 & \dots & 0 \end{bmatrix} \tag{9}$$

$$\sigma^* = \frac{RT}{L} \tag{10}$$

$$\mathbf{C}^* = \begin{bmatrix} \frac{T}{\rho J l}(c_1 + n_R^2 C_m)\frac{1}{\gamma_1} & -\frac{T}{\rho J l}c_1\frac{1}{\gamma_1} & 0 & \dots & 0 \\ -\frac{T}{\rho J l}c_1\frac{1}{\gamma_2} & \frac{T}{\rho J l}(c_1 + c_2)\frac{1}{\gamma_2} & -\frac{T}{\rho J l}c_2\frac{1}{\gamma_2} & \dots & 0 \\ 0 & -\frac{T}{\rho J l}c_2\frac{1}{\gamma_3} & \frac{T}{\rho J l}(c_2 + c_3)\frac{1}{\gamma_3} & \dots & 0 \\ \vdots & \vdots & \vdots & \ddots & \vdots \\ 0 & 0 & 0 & \dots & \frac{T}{\rho J l}c_{N-1}\frac{1}{\gamma_N} \end{bmatrix} \tag{11}$$

$$\mathbf{K}^* = \begin{bmatrix} \frac{1}{(x_2^*-x_1^*)}\frac{1}{\gamma_1} & -\frac{1}{(x_2^*-x_1^*)}\frac{1}{\gamma_1} & 0 & \dots & 0 \\ -\frac{1}{(x_2^*-x_1^*)}\frac{1}{\gamma_2} & \frac{1}{(x_2^*-x_1^*)}\frac{1}{\gamma_2} + \frac{1}{(x_3^*-x_2^*)}\frac{1}{\gamma_2} & -\frac{1}{(x_3^*-x_2^*)}\frac{1}{\gamma_2} & \dots & 0 \\ 0 & -\frac{1}{(x_3^*-x_2^*)}\frac{1}{\gamma_3} & \frac{1}{(x_3^*-x_2^*)}\frac{1}{\gamma_3} + \frac{1}{(x_4^*-x_3^*)}\frac{1}{\gamma_3} & \dots & 0 \\ \vdots & \vdots & \vdots & \ddots & \vdots \\ 0 & 0 & 0 & \dots & \frac{1}{(x_N^*-x_{N-1}^*)}\frac{1}{\gamma_N} \end{bmatrix} \tag{12}$$

2.2 Concentrated Parameters Optimization

A continuous model was proposed and analyzed initially to describe a slender shaft with some concentrated inertias. Based on it there was proposed a triple pendulum model to elaborate the optimization of the concentrated parameters. This pendulum is constituted by rotors with inertias $n_R^2 J_m$, J_2 and J_1, fixed to the metal shaft in the positions $x^* = 0$, $x^* = \overline{x}_1^* = l1/l$ and $x^* = 1$, respectively. From the continuous model using the torsional wave equation (Eq. (13)) and their boundary conditions (Eq. (14)) the dimensionless natural frequencies of the pendulum and modes of associated vibrations can be analytically calculated.

$$\frac{\partial^2\theta}{\partial t^{*2}} = \frac{\partial^2\theta}{\partial x^{*2}} \tag{13}$$

$$\begin{aligned} &(i) \quad \left.\frac{\partial\theta}{\partial x^*}\right|_{x^*=0} = \gamma_1 \left.\frac{\partial^2\theta}{\partial t^{*2}}\right|_{x^*=0} \\ &(ii) \quad -\left.\frac{\partial\theta}{\partial x^*}\right|_{x^*=\overline{x}_1^{*-}} + \left.\frac{\partial\theta}{\partial x^*}\right|_{x^*=\overline{x}_1^{*+}} = \gamma_{N1+1} \left.\frac{\partial^2\theta}{\partial t^{*2}}\right|_{x^*=\overline{x}_1^*} \\ &(iii) \quad \theta(x^* = \overline{x}_1^{*-}, t^*) = \theta(x^* = \overline{x}_1^{*+}, t^*) \\ &(iv) \quad -\left.\frac{\partial\theta}{\partial x^*}\right|_{x^*=1} = \gamma_N \left.\frac{\partial^2\theta}{\partial t^{*2}}\right|_{x^*=1} \end{aligned} \tag{14}$$

2.2.1 Continuous Model

The proposed continuous model in Eq. (13) and Eq. (14) accept a rigid body mode with natural frequency $\lambda_1 = 0$, whose associated normalized eigenmode is the constant function presented in Eq. (15).

$$\overline{\theta}_1(x^*) = \frac{1}{\sqrt{1 + \gamma_1 + \gamma_{N_1+1} + \gamma_N}} \tag{15}$$

The frequencies λ_j, $j = 2, 3, \ldots$, correspond to roots of Eq. (16), obtained from Eq. (13) and Eq. (14).

$$\cos(\lambda\overline{x}_1^*)\left(-1 - \frac{\gamma_{N_1+1}}{\gamma_1} + \frac{1}{\sigma(\lambda,\overline{x}_1^*)}\right) + \sin(\lambda\overline{x}_1^*)\left(-\frac{1}{\lambda\gamma_1} + \lambda\gamma_{N_1+1} - \frac{\beta(\lambda)}{\sigma(\lambda,\overline{x}_1^*)}\right) = 0 \tag{16}$$

The terms $\beta(\lambda)$ and $\sigma(\lambda, \overline{x}_1^*)$ were presented in Eq. (17) and Eq. (18), respectively.

$$\beta(\lambda) = \frac{\cos(\lambda) - \lambda\gamma_N \sin(\lambda)}{\sin(\lambda) + \lambda\gamma_N \cos(\lambda)} \tag{17}$$

$$\sigma(\lambda, \overline{x}_1^*) = \frac{\sin(\lambda\overline{x}_1^*) + \beta(\lambda)\cos(\lambda\overline{x}_1^*)}{\sin(\lambda\overline{x}_1^*) - \frac{1}{\lambda\gamma_1}\cos(\lambda\overline{x}_1^*)} \tag{18}$$

The first nine roots of Eq. (16) were enumerated in Tab.3.

Table 3. Natural frequencies of the system.

i	2	3	4	5	6	7	8	9	10
λ_i	0.0032	0.0083	4.3836	8.7672	11.0880	13.1509	17.5345	21.9181	22.1760
$f_i = \frac{\lambda_i}{2\pi T}$ (Hz)	0.7	1.7	910.5	1821.0	2303.0	2731.5	3642.0	4552.5	4606.1

eigenmodes associated to λ_j, $j = 2, 3, \ldots$ were shown in Eq. (19).

$$\phi_j(x^*) = \begin{cases} \sin(\lambda_j x^*) - \frac{1}{\lambda_j\gamma_1}\cos(\lambda_j x^*) & , 0 \leq x^* \leq \overline{x}_1^* \\ \frac{1}{\sigma(\lambda_j,\overline{x}_1^*)}\left[\sin(\lambda_j x^*) + \beta(\lambda_j)\cos(\lambda_j x^*)\right] & , \overline{x}_1^* \leq x^* \leq 1 \end{cases} \tag{19}$$

The norm of the modes in Eq. (19) was defined considering the inertia operator related to the weak formulation of the wave equation, Eq. (13) e Eq. (14). The inertia operator, the norms and the normalized eigenmodes for $j = 2, 3, \ldots$ were explained respectively in Eq. (20), Eq. (21) e Eq. (22).

$$\mathbf{M}(\phi_i, \phi_j) = \int_0^1 \phi_i\phi_j dx^* + \gamma_N\phi_i(1)\phi_j(1) + \gamma_{N_1+1}\phi_i(\overline{x}_1^*)\phi_j(\overline{x}_1^*) + \gamma_1\phi_i(0)\phi_j(0) \tag{20}$$

$$\|\phi_j\| = \sqrt{\mathbf{M}(\phi_j, \phi_j)} \tag{21}$$

$$\overline{\theta}_j(x^*) = \frac{\phi_j(x^*)}{\|\phi_j\|} \tag{22}$$

Equation (23) shows the final formulation of the continuous model of the triple pendulum, submitted to a concentrated generalized force F in any position x_F^* from the pendulum, where $\{\overline{\theta}(x_F^*)\} = \left[\overline{\theta}_1(x_F^*) \quad \overline{\theta}_2(x_F^*) \quad \cdots \quad \overline{\theta}_N(x_F^*)\right]^T$, $[D_c^*] = [d_{ij}]$ the damping matrix, with $d_{ij} = \frac{TD}{\rho J}\int_0^1 \overline{\theta}_i(x^*)\overline{\theta}_j(x^*)dx^*$, and $[K_c^*]$, described in Eq. (24), stiffness matrix. Variables ξ_j correspond to the generalized coordinates of the formulation of Lagrange for the continuous model (Hodges and Pierce, 2011), defined by Eq. (25).

$$\{\ddot{\xi}^*\} + [\mathbf{D_c^*}]\{\dot{\xi}^*(t^*)\} + [\mathbf{K_c^*}]\{\xi(t^*)\} = \frac{T^2}{\rho Jl}F(t^*T)\{\overline{\theta}(x_F^*)\} \tag{23}$$

$$[K_c^*] = \begin{bmatrix} \lambda_1^2 & 0 & 0 & \ldots & 0 \\ 0 & \lambda_2^2 & 0 & \ldots & 0 \\ 0 & 0 & \lambda_3^2 & \ldots & 0 \\ \vdots & \vdots & \vdots & \ddots & \vdots \\ 0 & 0 & 0 & \ldots & \lambda_N^2 \end{bmatrix} \tag{24}$$

$$\theta(x^*, t^*) = \sum_{j=1}^{N} \xi_j(t^*)\overline{\theta}_j(x^*) \tag{25}$$

2.2.2 Concentrated Parameters Model

A formulation similar to Eq. (23) was proposed for the model of concentrated parameters of the triple pendulum. In Eq. (26), Γ is a diagonal matrix whose elements are the dimensionless inertias γ_j, according to Eq. (27); F is a generalized force applied on the inertia rotor I_{i_F}; and $\mathbf{I}^{(\mathbf{N})}_{\mathbf{D_{i_F}}}$ is the i_F-th column of the identity matrix of dimension N. The matrices $[\mathbf{C}^*]$ and $[\mathbf{K}^*]$ had already been explained in Eq. (11) e Eq. (12), respectively.

$$\{\ddot{\theta}^*\} + [\mathbf{C}^*]\{\dot{\theta}^*(t^*)\} + [\mathbf{K}^*]\{\theta(t^*)\} = \frac{T^2}{\rho Jl} F(t^*T)\Gamma^{-1}\mathbf{I}^{(\mathbf{N})}_{\mathbf{D_{i_F}}} \tag{26}$$

$$\Gamma = \begin{bmatrix} \gamma_1 & 0 & 0 & \dots & 0 \\ 0 & \gamma_2 & 0 & \dots & 0 \\ 0 & 0 & \gamma_3 & \dots & 0 \\ \vdots & \vdots & \vdots & \ddots & \vdots \\ 0 & 0 & 0 & \dots & \gamma_N \end{bmatrix} \tag{27}$$

2.2.3 Optimization of Natural Frequencies

The objective of the first optimization was to obtain matrix $[\mathbf{K}^*]$ in a way to approximate as much as possible the natural frequencies of the model with concentrated parameters to the ones of the continuous model, whose frequencies were obtained analytically. The optimization was accomplished in Matlab, and the optimization method was the triangulation method, based on the objective function gradient.

The objective function to be optimized was defined as shown in Eq. (28), where λ_j are the frequencies obtained analytically and λ_{pc_j} the frequencies of the model with concentrated parameters.

$$\Psi_{obj}(x_2^*, \dots, x_{N_1}^*, x_{N_1+2}^*, \dots, x_{N-1}^*, \gamma_2, \dots, \gamma_{N_1}, \gamma_{N_1+2}, \dots, \gamma_{N-1}) = \left(\sum_{j=1}^{N} \left(\lambda_j^2 - \lambda_{pc_j}^2 \right)^2 \right)^{1/4} \tag{28}$$

As it can be noticed in Eq. (28), the variables referring to the position and inertia of the main rotors were kept fixed during optimization, in a way that $x_1^* = 0$, $x_{N_1+1}^* = \overline{x}_1^*$, $x_N^* = 1$, $\gamma_1 = \frac{n_R^2 J_m}{\rho Jl}$, $\gamma_{N_1+1} = \frac{J_2}{\rho Jl}$ and $\gamma_N = \frac{J_1}{\rho Jl}$. The initial values for the optimization variables were such that $x_i^* = (i-1)\frac{\overline{x}_1^*}{N_1}$, for $i = 2, \dots, N_1$, and for $i = N_1+2, \dots, N-1$, $x_i^* = (i - N_1 - 1)\frac{1-\overline{x}_1^*}{N-(N_1+1)}$, and $\gamma_j = \frac{\rho J(x_j - x_{j-1})}{\rho Jl} = x_j^* - x_{j-1}^*$, for $j = 2, 3, \dots, N_1, N_1+2, \dots, N-1$.

Table 4 shows the optimization result for different numbers of degrees of degree of freedom N, where $nConv$ correspond to the total number of iterations. A good agreement among natural frequencies for both models in study was noticed.

Table 4. Optimized Natural Frequencies for Different Numbers of Degrees of Degrees of Freedom.

λ_i	λ_1	λ_2	λ_3	λ_4	λ_5	λ_6	λ_7	λ_8	λ_9	$\Psi_{obj_{min}}$	n_{conv}
$N = 3$	0	0.0033	0.0083	–	–	–	–	–	–	$1.2 * 10^{-5}$	1
$N = 4$	0	0.0033	0.0083	4.3836	–	–	–	–	–	$1.0 * 10^{-5}$	282
$N = 5$	0	0.0033	0.0083	4.3836	8.7672	–	–	–	–	$1.0 * 10^{-5}$	465
$N = 6$	0	0.0033	0.0083	4.3836	8.7672	11.0880	–	–	–	$9.8 * 10^{-6}$	701
$N = 7$	0	0.0033	0.0083	4.3836	8.7672	11.0880	13.1509	–	–	$9.8 * 10^{-6}$	1098
$N = 8$	0	0.0033	0.0083	4.3836	8.7672	11.0880	13.1509	17.5345	–	$3.3 * 10^{-4}$	2001
$N = 9$	0	0.0033	0.0083	4.3836	8.7672	11.0880	13.1509	17.5345	21.9181	$9.7 * 10^{-6}$	2400
λ_{exact_i}	0	0.0033	0.0083	4.3836	8.7672	11.0880	13.1509	17.5345	21.9181	–	–

2.2.4 Optimization of Damping Coefficients

Once matrix $[\mathbf{K}^*]$ is obtained, the objective of the second optimization was the calculation of matrix $[\mathbf{C}^*]$, by means of an adjustment of the angular displacement curves of the main rotors in time. From the principle that the pendulum is a robust system, i.e., that its parameters are independent from the external forces to which the system is submitted, the curves for the optimization of angular displacement were obtained by means of the integration of Eq. (23) e Eq. (26), for $F(t^*T) = \delta(t^*)$, the unit impulse function, applied to the rotor J_2. For the numeric implementation, the unit impulse function was approximated according to Eq. (29), for $\epsilon = 0,001T$.

$$\delta(t^*) \approx \delta(t^*, \epsilon) = \begin{cases} \frac{1}{\epsilon} & , 0 \leq t^* \leq \epsilon \\ 0 & , t^* < 0 \quad \text{ou} \quad t^* > \epsilon \end{cases} \tag{29}$$

The objective function for the calculation of the damping coefficients c_j of the model of concentrated parameters was defined according Eq. (30), for $n_1 = 1$, $n_2 = N_1 + 1$ e $n_3 = N$.

$$\Phi_{obj}(c_1, \ldots, c_{N-1}) = \frac{1}{3} \sum_{j=1}^{3} \sqrt{\frac{1}{P^*} \int_0^{P^*} \left[\theta_{n_j}(t^*) - \theta(x^* = x^*_{n_j}, t^*)\right]^2 dt^*} \tag{30}$$

Table 5 shows optimization results for different values of degrees of freedom N, for $P = 3s$. The optimization was accomplished in Matlab, and the optimization method was the triangulation method, based on the objective function gradient.

Table 5. Damping Coefficient Optimimation.

c_i	c_1	c_2	c_3	$\Phi_{obj_{min}}$	n_{conv}
$N = 3$	0.0214	-0.0123	$-$	0.4210	51
$N = 4$	0.0361	0.0039	-0.0073	0.4577	181

3. TESTS

The proposed validation model test consisted in submitting the motor to a constant input voltage $v_A = 4V$, and in the clamping, in regime, of the rotor J_1 for $t = 1.2s$, leaving rotor J_2 free. The angular velocity curves of the motor and rotor J_1, obtained both in the numeric simulation (Eq. (1)), as well as in the experimental test were superimposed, as verified in Fig. 3 and Fig. 4.

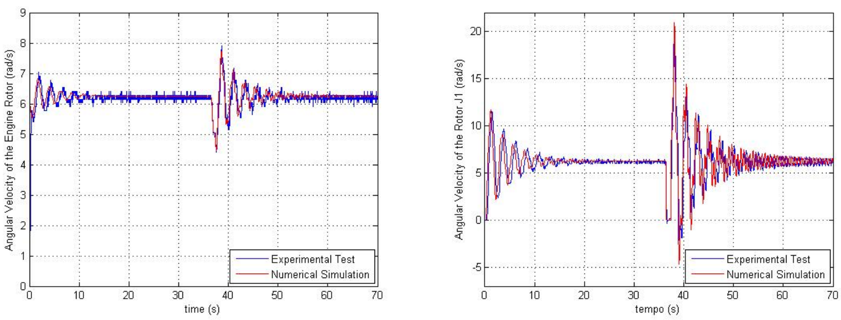

(a) (b)

Figure 3. System response in the time domain: (a) Angular speed of the drive rotor; (b) Angular speed of the rotor J_1

Initially there has been a great similarity between the angular velocity curves in time obtained from the proposed theoretical model and the experimental test. Figure 3a shows how the angular speed of the gearbox output varied with time. The vibrations at the begin of the motion and after the clamping of the rotor J_1 indicated that the participation of the motor in the dynamics of the coupled system was relevant. This fact motivated the study of the possibility of the inference of parameters related to the dynamic behavior of rotors J_1 e J_2 based on measurements performed on the motor. Figure 3b shows how the angular speed of the rotor J_1 varied with time and particularly the instant when the rotor was locked.

The frequency spectrum obtained from the angular speed of rotor J_1 (Fig. 4b) shows that the natural frequencies of the system were recovered by the proposed theoretical model.

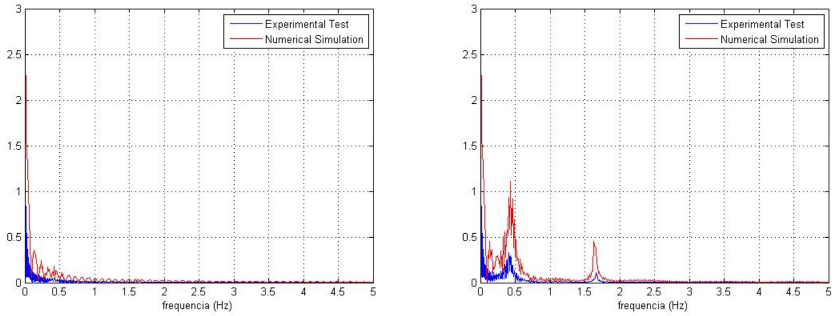

(a) (b)

Figure 4. System response in the frequency domain: (a) Spectrum obtained from the motor rotor signal; (b) Spectrum obtained from rotor J_1 signal

On the other hand, the natural frequencies are not so evident in the signal frequency spectrum measured at the output of the gearbox (Fig. 4a), which shows the information loss on the dynamic behavior of the rotors J_1 and J_2, considering only measurements made at the motor. This happened because of the energy dissipation which occurred along the shaft and due to the high dry friction acting in the motor.

4. CONCLUSIONS

An approach has been developed which seems most adequate for modeling the dynamics of a torsional system with a very slender shaft carrying some concentrated inertia and possible regions of contact with surrounding restraints. Basis of the analysis is the wave equation for the shaft considering regions of concentrated parameters. In parallel a discrete model of concentrated parameters is developed and it is fitted to the continuous approach using an optimization procedure. This investigation aims the development of tools to ease the possibility of detecting the position of rubbing, or other contact actions, occurring in a system with this kind of geometry. This will be the aim of a future research.

The analysis that was done in this preliminary investigation showed that the proposed approach produced satisfactory results when the system answers obtained from numerical simulation and experimental testing were confronted.

A hint to relevant aspects to be considered is that the angular velocity change at the drive output contains the information of the dynamics of the whole system, despite possible loss of energy due to dissipation. The approximated model developed according to the technique shown in this paper will possibly lead to conclusions on the open question of the disturbance position. This topic is of great interest, particularly for the oil industry, since it boasts not currently viable techniques for direct measurement parameters related to the interaction of the components of the drilling system with the rock.

5. REFERENCES

Andrade, B.C.C., 2013. *Numerical and experimental analysis of nonlinear torsional dynamics of a drilling system*. Master's thesis, Pontifícia Universidade Católica do Rio de Janeiro.

Franca, L.F.P., 2004. *Perfuração Percussiva-Rotativa Auto-Excitada em Rochas Duras*. Ph.D. thesis, Pontifícia Universidade Católica do Rio de Janeiro, Rio de Janeiro, Brazil.

Hodges, D.H. and Pierce, G.A., 2011. *Introduction to Structural Dynamics and Aeroelasticity*. Cambridge University Press, Georgia, 2nd edition.

Mihajlovic, N., 2005. *Torsional and Lateral Vibrations in Flexible Rotor Systems with Friction*. Ph.D. thesis, Technische Universiteit Eindhoven, Eindhoven.

Pogorelov, D., Mikheev, G., Lysikov, N., Ring, L., Gandikota, R. and Abedrabbo, N., 2012. "A multibody system approach to drill string dynamics modeling". In *Proceedings of the ASME 2012 11th Biennial Conference On Engineering Systems Disign And Analysis - ESDA2012*. Nantes, France.

6. RESPONSIBILITY NOTICE

The authors are the only responsible for the printed material included in this paper.